A Numerical Study of Line-Edge Roughness Scattering in Graphene Nanoribbons

Arash Yazdanpanah, Mahdi Pourfath, *Member, IEEE*, Morteza Fathipour, *Member, IEEE*, Hans Kosina, *Member, IEEE*, and Siegfried Selberherr, *Fellow, IEEE*

Abstract—The role of line-edge roughness scattering on the electronic properties of graphene nanoribbons is numerically investigated. The nonequilibrium Green function formalism, along with an atomistic tight-binding model, is employed. Our results indicate that, depending on the geometrical and roughness parameters, the transport of carriers can be in the diffusive or localization regime. We extract the mean free path and the localization length, which characterize the diffusive and localization regimes, respectively. In the diffusive regime, the conductance linearly decreases with length, whereas in the localization regime, it exponentially decreases with length. However, as the localization length depends on the carrier energy, an effective transport gap in this regime can be defined. This gap is evaluated as a function of the geometrical and roughness parameters, and its impact on the device performance is discussed.

Index Terms—Conductance, diffusive transport, effective band gap, graphene, localization, quantum transport.

I. INTRODUCTION

THE CONTINUED scaling of complementary metal–oxide–semiconductor transistors is limited due to various physical shortcomings such as short-channel effects, dielectric scaling, and leakage currents [1], [2]. To overcome these limitations, the introduction of novel materials such as compound semiconductors, carbon nanotubes, and graphene is investigated. Nowadays, single-layer graphene discovered in 2004 [3] has been identified as an ideal channel material in electronic applications [4]. High mobility at room temperature and at high doping concentrations [5], high thermal conductivity [6], and a width-dependent band gap [7] are some of the interesting properties of single-layer graphene. One of the problems that limit the application of graphene in electronic devices is the absence of an intrinsic band gap. In order to overcome this problem, graphene nanoribbons (GNRs) have been introduced, where
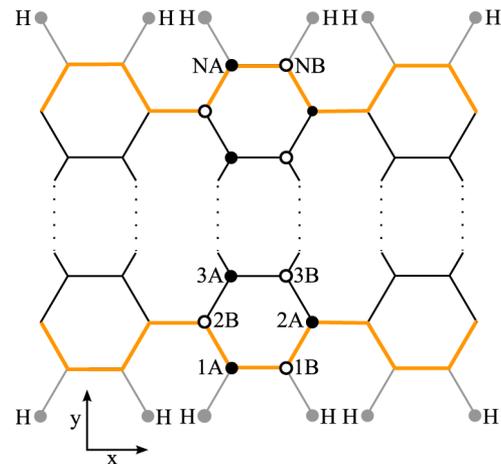
Fig. 1. Structure of a GNR with armchair edges.

graphene sheets are patterned into narrow ribbons [8]. With respect to the crystallographic direction, GNRs can be categorized as armchair, zigzag, or a combination of these two [9]. In this paper, we focus on armchair GNRs (see Fig. 1). The width of an armchair GNR is given by $W = (N+1)(\sqrt{3}/2)a_{cc}$, where N is the number of carbon atoms along the width direction and $a_{cc} = 1.42$Å is the distance between nearest-neighbor carbon atoms. In armchair GNRs, the band gap is inversely proportional to the width. A band gap suitable for electronic applications can be achieved by making sufficiently narrow GNRs [7]. The electronic transport properties of GNRs have been recently studied in several experimental works [7], [8], [10]. The results indicate that line-edge roughness scattering is the dominant scattering mechanism in narrow GNRs [11]. The effect of line-edge roughness on transport in GNRs has been numerically studied in [12]–[15] where the electronic band structure is described using a first-nearest-neighbor tight-binding model and edge roughness is modeled by assuming that atoms at the edges are randomly removed with uniform probability, neglecting the correlation between edges. First-nearest-neighbor tight-binding calculations predict that one third of all armchair GNR configurations are metallic [16], [17]. However, both experimental data [7], [8], [10] and *ab initio* calculations [18]–[20] show that all narrow armchair GNRs have a finite band gap. A tight-binding model can accurately describe the electronic band structure of GNRs only if the interaction up to third nearest neighbors are considered [20], [21]. Therefore, in this paper, a three-nearest-neighbor tight-binding model is employed. To model line-edge roughness in a more realistic way [22], we assume an exponential autocorrelation between

edge disorders [23], [24]. Employing the nonequilibrium Green function (NEGF) formalism, the conductance of GNRs is studied in both the diffusive and localization regimes. The effect of localization is investigated in terms of an effective transport gap, which is strongly affected by the geometrical and roughness parameters. This paper is organized as follows: In Section II the tight-binding model, the NEGF formalism, the line-edge roughness model, and the diffusive and localization regimes are discussed. The role of geometrical and roughness parameters are investigated in Section III. Finally, concluding remarks are presented in Section IV.

II. MODEL AND METHODS

A. Tight-Binding Model

GNRs can be considered as a graphene sheet tailored along a certain direction and can be accordingly classified as of armchair or zigzag shape, or a combination of these two. The GNR lattice consists of two sublattices A and B (see Fig. 1). The unit cell of an armchair GNR contains n A-type and n B-type carbon atoms. A first-nearest-neighbor tight-binding model is commonly used to model the band structure of GNRs [25]. However, in this paper, a third-nearest-neighbor tight-binding model has been employed [21], [26], which yields a more accurate dispersion relation and predicts a nonzero band gap for all armchair edge GNRs [21], i.e.,

$$H = H_1 + H_3. \tag{1}$$

Here, H_1 and H_3 represent the first- and third-nearest-neighbor Hamiltonians, respectively. These Hamiltonians can be expressed in terms of creation and annihilation operators $a^\dagger$ and a, respectively, which act on the π state on each site, i.e.,

$$H_1 = \sum_{\langle i,j \rangle} t_{i,j} a_i^\dagger a_j \tag{2}$$

$$H_3 = \sum_{\langle i,m \rangle} t_{i,m} a_i^\dagger a_k. \tag{3}$$

Here, $t_{i,j} \approx -3.2$ eV and $t_{i,m} \approx -0.3$ eV are the hopping parameters between the first and third nearest neighbors, respectively. The summation of i runs over the entire nanoribbon lattice, whereas j and m are restricted to the first and third nearest neighbors to site i, respectively.

B. Line-Edge Roughness

Both experimental data [11] and theoretical predictions [15], [27]–[29] indicate that the line-edge roughness is the dominant source of scattering in narrow GNRs. Line-edge roughness is a statistical phenomenon that can be well described by means of an autocorrelation function [23]. Commonly, a Gaussian or exponential autocorrelation is assumed to describe line-edge roughness. The exponential correlation function gives a rougher edge than the Gaussian correlation function with the same parameter values [23]. Short wavelength fluctuations of the edge arise from the high frequency tail of the exponential power

spectrum [30]. In this paper, an exponential autocorrelation is applied, i.e.,

$$R(x) = \Delta W^2 \exp\left(-\frac{|x|}{\Delta L}\right), \qquad x = n\Delta x \tag{4}$$

where ΔW is the root mean square of the fluctuation amplitude, ΔL is the roughness correlation length that is a measure of smoothness, and Δx is the sampling interval chosen equal to $a_{cc}/2$. To create line-edge roughness in real space, we first evaluate the Fourier transform of the autocorrelation, which gives the power spectrum of the roughness. By applying a random phase to the power spectrum followed by an inverse Fourier transform, roughness in real space is achieved [24]. We create many samples with the same roughness parameters and evaluate their electronic properties. Finally, statistical averaging on these samples is performed.

C. NEGF Formalism

NEGFs provide a powerful technique for the analysis of nanoscale devices [31]–[33]. The system under consideration is composed of a channel that is connected to two leads. The retarded Green function G_D of the channel can be obtained as

$$G_D = [(E + i\eta)I - H_D - \Sigma_L - \Sigma_R]^{-1} \tag{5}$$

where η is an infinitesimally small quantity and H_D is the Hamiltonian of the device, which can be evaluated using a tight-binding model as explained before. Σ_L and Σ_R are the contact self-energy functions describing the broadening and the shift of the energy levels due to the interaction with the left and right contacts, respectively, and can be obtained as

$$\Sigma_L = \beta_L^\dagger g_L \beta_L \quad \Sigma_R = \beta_R g_R \beta_R^\dagger. \tag{6}$$

Here, g_L and g_R are the surface Green functions of the left and right contacts, respectively, and β_L and β_R are the coupling matrices between the device and the respective contact. The surface Green functions of the contacts can be efficiently calculated using an iterative scheme [34]. The transmission probability of carriers through the device can be evaluated as [35]

$$T(E) = \text{Trace}\left[\Gamma_L G_D \Gamma_R G_D^\dagger\right]. \tag{7}$$

Γ is the contact-broadening function defined as

$$\Gamma_{L,R} = i\left[\Sigma_{L,R} - \Sigma_{L,R}^\dagger\right]. \tag{8}$$

Finally, in the linear response regime, the conductance of a nanoribbon can be calculated as

$$G(E) = G_0 T(E)\left(-\frac{\partial f}{\partial E}\right) \tag{9}$$

with $G_0 = 2q^2/h$.

D. *Diffusive and Localization Regimes*

In the absence of scattering, the carrier transport is in the ballistic regime where the conductance is independent of the device length. In the presence of scattering, the transport of carriers is in the diffusive regime, where the transmission can be written as

$$\langle T(E) \rangle = \frac{N_{\text{ch}}}{1 + L/\lambda(E)}. \tag{10}$$

Here, $\lambda(E)$ is the mean free path, N_{ch} is the number of active conduction channels, and L is the length of the ribbon. Therefore, the conductance in the diffusive regime is inversely proportional to the device length, i.e.,

$$G(E) \approx G_0 \frac{N_{\text{ch}}}{1 + L/\lambda(E)} \left(-\frac{\partial f}{\partial E} \right). \tag{11}$$

For phase-coherent transport, in the presence of disorder, the carrier wave function can be scattered back and forth between potential barriers, and standing waves along the device form. In this regime, referred to as the localization regime, the transport of carriers is due to tunneling between localized states, and the average transmission probability exponentially decreases with the device length [36], i.e.,

$$\langle \ln T(E) \rangle \approx -L/\xi(E) \tag{12}$$

where $\xi(E)$ is the localization length. In the localization regime, the conductance can be obtained as [37]

$$G(E) \approx G_0 \exp\left[-\frac{L}{\xi(E)} \right] \left(-\frac{\partial f}{\partial E} \right). \tag{13}$$

In this paper, the carrier mean free path and localization length are evaluated from numerical simulations. The mean free path can be obtained by fitting a linear function to the inverse of the average transmission in the diffusive regime, i.e., $1/\langle T(E) \rangle = 1/N_{\text{ch}} + L/(N_{\text{ch}}\lambda)$. In the localization regime, the transmission probability exponentially decreases with the length. Therefore, the slope of the transmission probability as a function of length in the logarithmic scale is inversely proportional to the localization length.

III. NUMERICAL RESULTS

Here, the effect of the geometrical and roughness parameters on the transmission probability, the conductance, and the effective transport gap of GNRs is investigated. The mean free path and the localization length as a function of the geometrical and roughness parameters are extracted. Finally, the performance of GNR field-effect transistors (FETs) in the presence of line-edge roughness is investigated.

A. *Role of the Device Length*

The transmission probability for many samples and the average transmission probability for different lengths are shown in Fig. 2. With increasing the ribbon's length, the average transmission probability is reduced. Furthermore, as the length in-
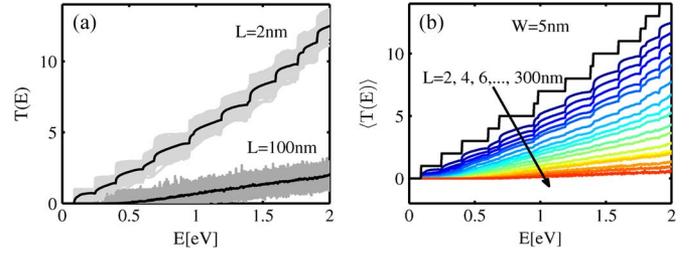

Fig. 2. (a) (Solid-black line) The average transmission probability over different samples and (gray lines) the transmission probability of each sample as a function of energy at $L = 2$ nm and $L = 10$ nm. (b) Comparison between the average transmission probabilities as a function of energy at various lengths. For all devices, $\Delta L = 3$ nm, and $\Delta W/W = 2\%$.
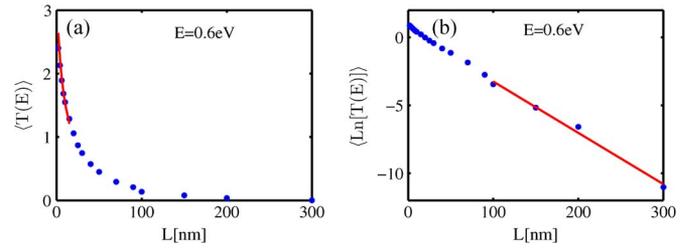

Fig. 3. (a) The average transmission probability as a function of length. (b) The average of the logarithm of the transmission probability as a function of length. $W = 5$ nm, $\Delta W/W = 2\%$, and $\Delta L = 3$ nm. The solid lines show the fitted curves to the average transmission probability and logarithm of the transmission probability. According to fitted data, the mean free path is $\lambda \approx 10$ nm, and the localization length is $\xi \approx 30$ nm. The ratio of the localization length and the mean free path is equal to the number of available channels at this energy ($N_{\text{channel}} = 3$).

creases, the steps in the transmission probability are smoothed out. To discriminate the diffusive and localization transport regimes, the average transmission probabilities $\langle T(E) \rangle$ and $\langle \ln(T(E)) \rangle$ as a function of length at $E = 0.6$ eV are shown in Fig. 3. In short ribbons, the average transmission is inversely proportional to the length (diffusive regime), but for longer ribbons, the transmission probability exponentially decreases with the length. In the diffusive regime, one can obtain the mean free path $\lambda(E)$ by fitting a curve similar to (10) to the average transmission probability [see Fig. 3(a)]. If $L \ll \lambda$, the transport is ballistic. In the localization regime where the transmission probability exponentially decreases with the length, one can obtain the localization length $\xi(E)$ by fitting a curve similar to (12) [see Fig. 3(b)]. For $L \ll \xi$, the transport will be diffusive. At $E = 0.6$ eV, the mean free path can be estimated as $\lambda \approx 10$ nm, and the localization length is $\xi \approx 30$ nm. It can be shown that the ratio of the localization length to the mean free path is proportional to the number of available subbands [38], i.e.,

$$\frac{\xi}{\lambda} \propto N_{\text{ch}}(E). \tag{14}$$

For the discussed sample at $E = 0.6$ eV, this ratio is 3, which is exactly the number of available subbands at this energy. Fig. 4 shows the estimated mean free path and the localization length as a function of energy for $W = 5$ nm and $W = 7.5$ nm. The elastic mean free path in the energy interval of each subband increases, but it decreases at the beginning of the next subband because the scattering rate increases at the edge of subbands
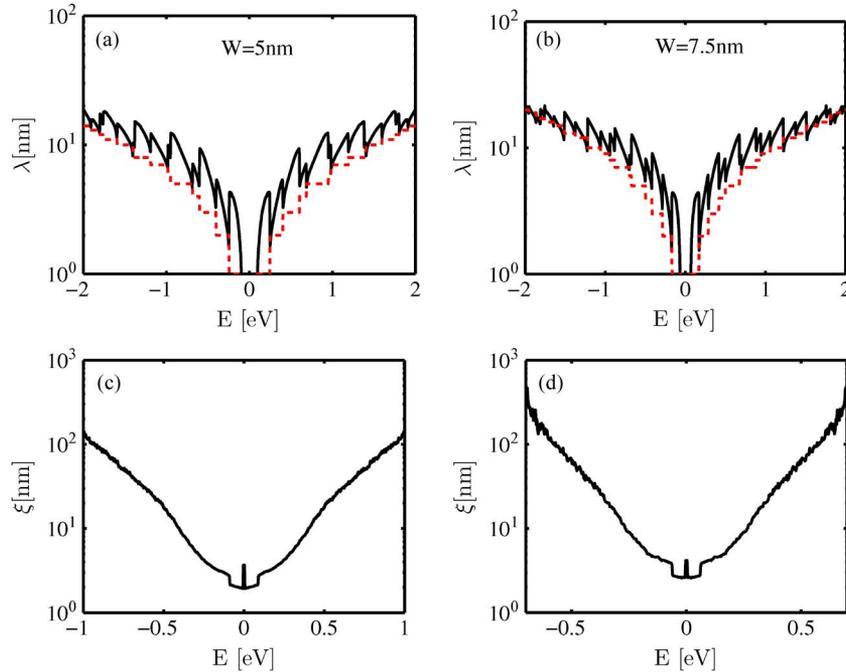
Fig. 4.   (Solid-black line) Mean free path and (dashed-red line) ballistic transmission probability as a function of energy for (a) $W = 5$ nm and (b) $W = 7.5$ nm. Localization length as a function of energy at (c) $W = 5$ nm and (d) $W = 7.5$ nm. $\Delta L = 3$ nm, and $\Delta W/W = 2\%$.
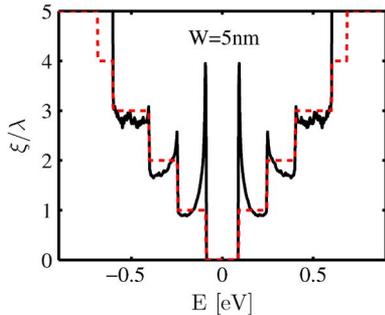

Fig. 5.   (Solid-black line) Ratio of the localization length and the mean free path as a function of energy. (Dashed-red line) Available conducting channel at each energy. $\Delta L = 3$ nm, and $\Delta W/W = 2\%$.
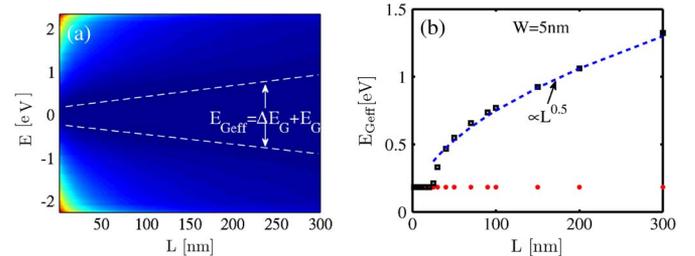

Fig. 6.   (a) Average transmission probability as a function of energy and length. (Dashed lines) Border of the region where the transmission is smaller than 10^{-2}, where we defined it as the effective band gap in presence of edge roughness. (b) Comparison between (rectangles) the effective transport band gap and (circles) the band structure gap. (Dashed line) Scaling of the effective band gap versus length. $\Delta L = 3$ nm, and $\Delta W/W = 2\%$.

as result of the Van Hove singularities in the density of states. According to this figure, we find that the localization length becomes shorter, as the width of the ribbon decreases. This width dependence of the localization length suggests that edge disorder plays an important role on the carrier localization in narrow GNRs.

Fig. 5 shows that ratio (14) is more or less equal to the number of the conducting channels at the respective energies. Fig. 6(a) shows the transmission probability as a function of length and energy. Due to a shorter localization length at low energies, the transmission probability is strongly suppressed, particularly at long channel lengths. To quantify the role of localization on the transport properties, we define an effective transport gap ($E_{\text{Geff}} = \Delta E_G + E_G$), where the transmission probability drops to values below 10^{-2}, indicated by the white dashed lines in Fig. 6(a). The effective transport gap for a 5-nm-wide GNR as a function of length is compared with the band structure gap in Fig. 6(b). Apparently, the effective transport gap increases with the length of the sample, where transport

takes place in the localization regime ($L \geq 20$ nm). In this regime, the effective transport gap is proportional to $L^{1/2}$, which is consistent with the analytical model proposed in [39] [see (15) in the Appendix].

The conductance of nanoribbons versus the length for different widths but with the same roughness percentage is plotted in Fig. 7 in logarithmic scale. As the device length becomes larger than the localization length, one gets into the localization regime, where the conductance exponentially decreases with the length. This figure shows that, by increasing the width, localization occurs at longer lengths. As the width of the ribbon increases, the number of available channels and, as a result, the localization length increase [see (14)].

B. Role of the Width

Fig. 8(a) compares the transmission probabilities of perfect and rough GNRs for different widths. Apparently, the steps of
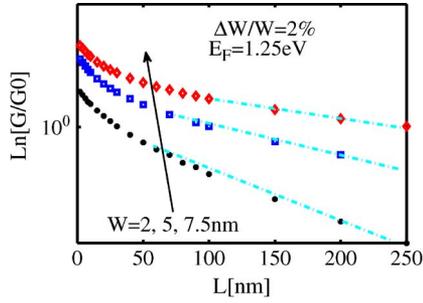
Fig. 7. Logarithm of average conductance as a function of length at various widths but with the same roughness amplitude percent. (Dashed lines) Fitted exponential curves to the simulation results. $\Delta L = 3$ nm.
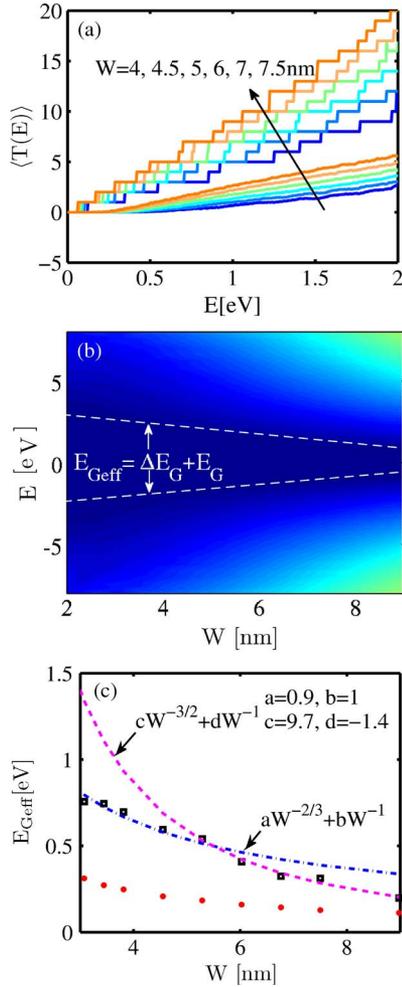

Fig. 8. (a) Comparison between the average transmission probabilities of rough GNRs with that of GNRs with perfect edges. (b) The average transmission probability as a function of energy and width. (Dashed lines) Border of the region where the transmission is smaller than 10^{-2}. (c) The effective transport gap and the corresponding fitted curves are compared with the band structure gap as a function of width. For all devices, $\Delta L = 3$ nm, $\Delta W/W = 2\%$, and $L = 50$ nm.

Fig. 9. (a) Comparison between the average conductance as a function of width employing quantum–mechanical simulations (QM) and semiclassical calculations (SC). E_C is the energy difference between the conduction-band edge and the Dirac point of the underlying graphene band structure.

transport gap is even more increased due to the localization of carriers, particularly at low energies. This can be better understood by considering the region where the average transmission probability is smaller than 10^{-2} [dark blue region in Fig. 8(b)]. The effective transport gap (rectangles) and the band structure gap (circles) as a function of the width are shown in Fig. 8(c). For narrow ribbons, there are only few available conducting channels so that the localization length will be shorter and the effective transport gap will be larger. The effective transport gap scales with the width as $aW^{-2/3} + bW^{-1}$ (dash-dot line) for narrow ribbons and with $cW^{-3/2} + dW^{-1}$ (dashed line) for wider ribbons. These results are in agreement with the analytical model that we derived in [39]. It can be shown that the effective transport gap will be proportional to $\Delta E_G \propto (m^* E_G^2)^{1/2}$ for wide ribbons and $\Delta E_G \propto (E_G)^{2/3}$ for narrow ribbons. As the effective mass and the band structure gap of the ribbon are inversely proportional to the width, ΔE_G is expected to scale with $W^{-3/2}$ for wide ribbons and with $W^{-2/3}$ for narrow ribbons.

Fig. 9(a) compares the conductance obtained from the semiclassical model derived in [39] with the quantum–mechanical simulations that we performed in this paper. Both methods predict that the conductance linearly scales with W; however, the conductance obtained from the quantum–mechanical simulations is about a factor of two smaller than that obtained from the semiclassical model. This is due to a lager transmission obtained from the perturbation method in comparison with the atomistic model, where the carbon atoms removed from the edges are treated by setting the appropriate hopping elements of the Hamiltonian to zero.

C. Role of the Roughness Amplitude

As roughness increases, the average transmission probability of GNRs can be significantly reduced, and the transport regime changes from the diffusive regime to the localization regime. For a better comparison, the average transmission probability as a function of energy and roughness amplitude is shown in Fig. 10(a). A comparison between the effective transport gap and the band structure gap is shown in Fig. 10(b). The figure shows that the effective transport gap significantly increases with roughness amplitudes larger than 0.5%, due to

the transmission probability of GNRs with perfect edges are smoothed out in the presence of line-edge roughness.

Fig. 8(b) shows the average transmission probability as a function of width and energy for GNRs with $L = 50$ nm. In the absence of disorder, the band gap of the ribbons increases as the width decreases, but in the presence of edge disorder, the
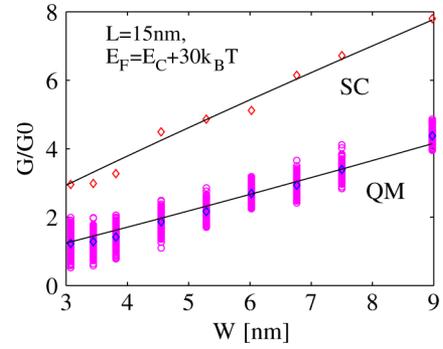
Fig. 10.   (a) Average transmission probability as a function of energy and roughness amplitude. (Dashed lines) Effective transport gap. (b) The effective transport gap and the band structure gap as a function of roughness amplitude. $\Delta L = 3$ nm.

Fig. 11.   Logarithm of the average conductance as a function of the roughness amplitude at $L = 20$ nm and $L = 50$ nm.
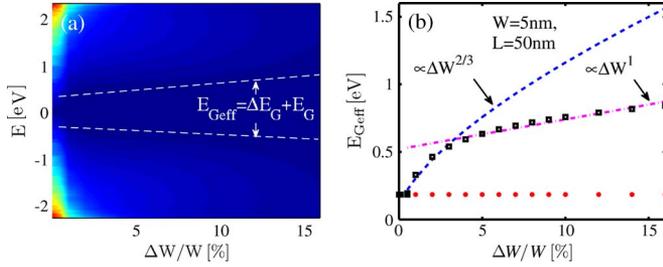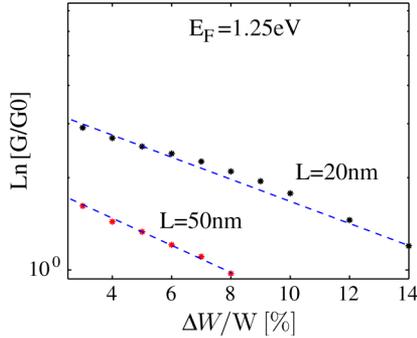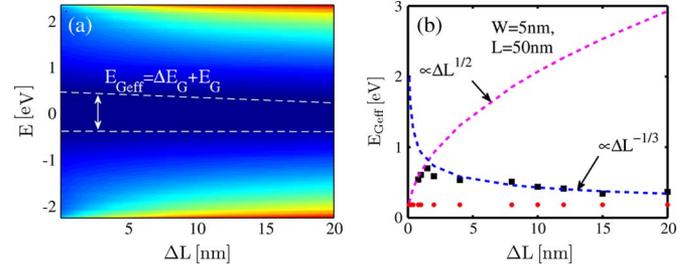

Fig. 12.   (a) Average transmission probability as a function of energy and roughness amplitude. (Dashed lines) Effective transport gap. (b) The effective transport gap and the band structure gap as a function of the correlation length. $\Delta W/W = 2\%$.
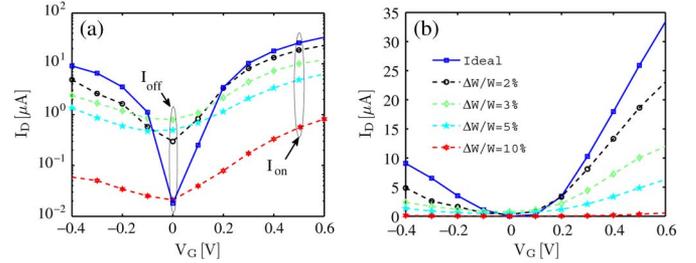

Fig. 13.   Ensemble average of the transfer characteristics in (a) logarithmic and (b) linear scales. $W = 1.6$ nm, $L = 20$ nm, and $\Delta L = 10$ nm.

the formation of localized states across the ribbon. With the further increase in the line-edge roughness, localized states get extended over the entire width and thus block the conductive paths. Therefore, the transmission probability decreases, and the effective transport gap increases. Fig. 10(b) shows that the effective transport gap scales with $\Delta W^{2/3}$ and ΔW^1 for smooth and rough edges, respectively. These results are in agreement with the analytical model in (15). As a result of the effective transport gap increase, the conductance exponentially decreases (see Fig. 11).

D. Role of the Correlation Length

The average transmission probability as a function of energy and correlation length is plotted in Fig. 12(a). The results indicate that the average transmission probability increases as the correlation length increases and that the respective effective transport gap decreases. At longer correlation lengths, the line-edge roughness becomes smoother, which results in a longer mean free path and localization length. For the given structure, the effective transport gap and the energy gap are shown in Fig. 12(b). With increasing correlation length, the effective transport gap increases first and then decreases. The length dependences of the effective transport gap are $\Delta L^{1/2}$ and $\Delta L^{-1/3}$, respectively [see (15)]. This behavior can be understood by considering the de Broglie wavelength of electrons. When it becomes comparable with the roughness correlation length of the ribbon, the scattering rate will be maximized [39]. As a result, the effective transport gap peaks at this point.

E. Device Performance

Here, we investigate the role of roughness on the transfer characteristics of GNR-FETs. The length and the width of the simulated structure are chosen to be $L = 20$ nm and $W = 1.6$ nm, respectively. A top gate geometry, along with a 1.5-nm Al_2O_3 gate dielectric are assumed. We simulated 200 different samples with the same geometrical and roughness parameters and took an ensemble average over their characteristics. Fig. 13(a) and (b) compare the transfer characteristics at various roughness amplitudes in logarithmic and linear scales, respectively. At small roughness, the off-current increases with the roughness amplitude. This behavior is related to the formation of some localized states in the band gap [40]. The band-to-band tunneling of carriers is strongly enhanced in the presence of such states, and as a result, the off-current increases. With the increase in the off-current, the device performance in terms of the I_{on}/I_{off} ratio and the subthreshold slope is degraded. As roughness further increases, however, the off-current decreases. This behavior is due to the increase in the transport band gap. As we mentioned before, the effective transport gap increases with the roughness amplitude, and as result, the current decreases. In the case of strong roughness, the increase in the transport gap dominates of the effects of gap states, and both the on- and off-currents decrease.

IV. CONCLUSION

Using a three-nearest-neighbor tight-binding model, along with a realistic model for edge disorder, we have investigated the electronic properties of armchair edge GNRs in the presence of line-edge roughness. We have studied the transport properties of GNRs in both the diffusive and localization regimes and extracted the mean free path and the localization length.

Line-edge roughness can induce quasi-localized states, particularly in narrow ribbons. The localization of carriers reduces the transmission probability at energies close to the band edge, and the effective transport gap in such devices increases. The numerical results presented in this paper verify the accuracy of the analytical model that we derived before, which is useful for a better understanding of the transport properties of nanoribbons and for the design of graphene-based devices.

APPENDIX

In our previous work [39], we showed that ΔE_G induced by the localization of carriers due to the presence of line-edge roughness can be approximated by

$$
\Delta E_G = \begin{cases} 2\left(\frac{k_B T L}{C}\right)^{1/2} & D \ll \left(\frac{C}{k_B T L}\right)^{1/2} \\ 2\left(\frac{2k_B T L}{CD}\right)^{1/3} & D \gg \left(\frac{C}{2k_B T L}\right)^{1/2} \end{cases} \tag{15}
$$

with

$$
C = \left(\frac{W}{\Delta W}\right)^2 \frac{\hbar^2}{2m^* \Delta L E_G^2} \tag{16}
$$

$$
D = \frac{8m^* \Delta L^2}{\hbar^2}. \tag{17}
$$

For wide ribbons, the first condition is satisfied, and the second one is satisfied for narrow ribbons. In (16) and (17), m^*, E_G, and L are the effective mass, the band structure gap, and the device length, respectively.

REFERENCES

[1] W. Kim, K. T. Do, and Y. H. Kim, "Statistical leakage estimation based on sequential addition of cell leakage currents," *IEEE Trans. Very Large Scale Integr. (VLSI) Syst.*, vol. 18, no. 4, pp. 602–615, Apr. 2010.

[2] G. Q. Lo, A. B. Joshi, and D. Kwong, "Hot-carrier-stress effects on gate-induced drain leakage current in n-channel MOSFETs," *IEEE Electron Device Lett.*, vol. 12, no. 1, pp. 5–7, Jan. 1991.

[3] K. Novoselov, A. Geim, S. Morozov, D. Jiang, Y. Zhang, S. Dubonos, I. Grigorieva, and A. Firsov, "Electric field effect in atomically thin carbon films," *Science*, vol. 306, no. 5696, pp. 666–669, Oct. 2004.

[4] Y.-M. Lin, K. Jenkins, A. Valdes-Garcia, J. Small, D. Farmer, and P. Avouris, "Operation of graphene transistors at GHz frequencies," *Nano Lett.*, vol. 9, no. 1, pp. 422–426, 2009.

[5] F. Schedin, A. K. Geim, S. V. Morozov, E. W. Hill, P. Blake, M. I. Katsnelson, and K. S. Novoselov, "Detection of individual gas molecules adsorbed on graphene," *Nat. Mater.*, vol. 6, no. 9, pp. 652–655, Sep. 2007.

[6] A. A. Balandin, S. Ghosh, W. Bao, I. Calizo, D. Teweldebrhan, F. Miao, and C. N. Lau, "Superior thermal conductivity of single-layer graphene," *Nano Lett.*, vol. 8, no. 3, pp. 902–907, Mar. 2008.

[7] M. Han, B. Özyilmaz, Y. Zhang, and P. Kim, "Energy band-gap engineering of graphene nanoribbons," *Phys. Rev. Lett.*, vol. 98, no. 20, pp. 206 805-1–206 805-4, May 2007.

[8] Z. Chen, Y. Lin, M. Rooks, and P. Avouris, "Graphene nano-ribbon electronics," *Phys. E*, vol. 40, no. 2, pp. 228–232, Dec. 2007.

[9] P. Koskinen, S. Malola, and H. Häkkinen, "Evidence for graphene edges beyond zigzag and armchair," *Phys. Rev. B*, vol. 80, no. 7, pp. 073 401-1–073 401-3, Aug. 2009.

[10] X. Li, L. Zhang, S. Lee, and H. Dai, "Chemically derived, ultrasmooth graphene nanoribbon semiconductors," *Science*, vol. 319, no. 5867, pp. 1229–1232, Feb. 2008.

[11] Y. Yang and R. Murali, "Impact of size effect on graphene nanoribbon transport," *IEEE Electron Device Lett.*, vol. 31, no. 3, pp. 237–239, Mar. 2010.

[12] Y. Yoon and J. Guo, "Effect of edge roughness in graphene nanoribbon transistors," *Appl. Phys. Lett.*, vol. 91, no. 7, pp. 073 103-1–073 103-3, Aug. 2007.

[13] G. Fiori and G. Iannaccone, "Simulation of graphene nanoribbon field-effect transistors," *IEEE Electron Device Lett.*, vol. 28, no. 8, pp. 760–762, Aug. 2007.

[14] A. Lherbier, B. Biel, Y. Niquet, and S. Roche, "Transport length scales in disordered graphene based materials: Strong localization regime and dimensionality effects," *Phys. Rev. Lett.*, vol. 100, no. 3, pp. 036 803-1–036 803-4, Jan. 2008.

[15] E. R. Mucciolo, A. H. C. Neto, and C. H. Lewenkopf, "Conductance quantization and transport gaps in disordered graphene nanoribbons," *Phys. Rev. B*, vol. 79, no. 7, pp. 075 407-1–075 407-3, Feb. 2009.

[16] M. Ezawa, "Peculiar width dependence of the electronic properties of carbon nanoribbons," *Phys. Rev. B*, vol. 73, no. 4, pp. 045 432-1–045 432-8, Jan. 2006.

[17] L. Brey and H. Fertig, "Electronic states of graphene nanoribbons studied with the Dirac equation," *Phys. Rev. Lett.*, vol. 73, no. 23, pp. 235 411-1–235 411-5, Jun. 2006.

[18] Y.-W. Son, M. Cohen, and S. Louie, "Energy gaps in graphene nanoribbons," *Phys. Rev. Lett.*, vol. 97, no. 21, pp. 216 803-1–216 803-4, Nov. 2006.

[19] V. Barone, O. Hod, and G. E. Scuseria, "Electronic structure and stability of semiconducting graphene nanoribbons," *Nano Lett.*, vol. 6, no. 12, pp. 2748–2754, Dec. 2006.

[20] C. T. White, J. Li, D. Gunlycke, and J. W. Mintmire, "Hidden one-electron interactions in carbon nanotubes revealed in graphene nanostrips," *Nano Lett.*, vol. 7, no. 3, pp. 825–830, Mar. 2007.

[21] D. Gunlycke and C. T. White, "Tight-binding energy descriptions of armchair-edge graphene nanostrips," *Phys. Rev. B*, vol. 77, no. 11, pp. 115 116-1–115 116-6, Mar. 2008.

[22] G. Xu, C. M. Torres, Jr., J. Bai, J. Tang, T. Yu, Y. Huang, X. Duan, Y. Zhang, and K. L. Wang, "Linewidth roughness in nanowire-mask-based graphene nanoribbons," *Appl. Phys. Lett.*, vol. 98, no. 24, pp. 243 118-1–243 118-3, Jun. 2011.

[23] S. M. Goodnick, D. K. Ferry, C. W. Wilmsen, Z. Liliental, D. Fathy, and O. L. Krivanek, "Surface roughness at the Si(100)- SiO₂ interface," *Phys. Rev. B*, vol. 32, no. 12, pp. 8171–8186, Dec. 1985.

[24] J. Wu, "Simulation of non-Gaussian surfaces with FFT," *Tribol. Int.*, vol. 37, no. 4, pp. 339–346, Apr. 2004.

[25] H. Zheng, Z. Wang, T. Luo, Q. Shi, and J. Chen, "Analytical study of electronic structure in armchair graphene nanoribbons," *Phys. Rev. B*, vol. 75, no. 16, pp. 165 414-1–165 414-6, Apr. 2007.

[26] S. Reich, J. Maultzsch, C. Thomsen, and P. Ordejón, "Tight-binding description of graphene," *Phys. Rev. B*, vol. 66, no. 3, pp. 035 412-1–035 412-5, Jul. 2002.

[27] D. Areshkin, D. Gunlycke, and C. White, "Ballistic transport in graphene nanostrips in the presence of disorder: Importance of edge effects," *Nano Lett.*, vol. 7, no. 1, pp. 204–210, Jan. 2007.

[28] D. Gunlycke, D. Areshkin, and C. White, "Semiconducting graphene nanostrips with edge disorder," *Appl. Phys. Lett.*, vol. 90, no. 14, pp. 142 104-1–142 104-3, Apr. 2007.

[29] M. Evaldsson, I. V. Zozoulenko, H. Xu, and T. Heinzel, "Edge-disorder-induced anderson localization and conduction gap in graphene nanoribbons," *Phys. Rev. B*, vol. 78, no. 16, pp. 161 407(R)-1–161 407(R)-4, Oct. 2008.

[30] J. A. Ogilvy and J. R. Foster, "Rough surfaces: Gaussian or exponential statistics," *J. Phys. D, Appl. Phys.*, vol. 22, no. 9, pp. 1243–1251, Sep. 1989.

[31] G. Klimeck, S. S. Ahmed, N. Kharche, M. Korkusinski, M. Usman, M. Prada, and T. B. Boykin, "Atomistic simulation of realistically sized nanodevices using NEMO 3-D Part I: Models and benchmarks," *IEEE Trans. Electron Devices*, vol. 54, no. 9, pp. 2079–2089, Sep. 2007.

[32] G. Klimeck, S. S. Ahmed, N. Kharche, M. Korkusinski, M. Usman, M. Prada, and T. B. Boykin, "Atomistic simulation of realistically sized nanodevices using NEMO 3-D Part II: Applications," *IEEE Trans. Electron Devices*, vol. 54, no. 9, pp. 2090–2099, Sep. 2007.

[33] M. P. Anantram and A. Svizhenko, "Multidimensional modelling of nanotransistors," *IEEE Trans. Electron Devices*, vol. 54, no. 9, pp. 2100–2115, Sep. 2007.

[34] M. P. L. Sancho, J. M. L. Rubio, and L. Rubio, "Highly convergent schemes for the calculation of bulk and surface green functions," *J. Phys. F, Metal Phys.*, vol. 15, no. 4, pp. 851–858, Apr. 1985.

[35] Y. Meir and N. S. Wingreen, "Landauer formula for the current through an interacting electron region," *Phys. Rev. Lett.*, vol. 68, no. 16, pp. 2512–2515, Apr. 1992.

[36] P. Anderson, D. Thouless, E. Abrahams, and D. Fisher, "New method for a scaling theory of localization," *Phys. Rev. B*, vol. 22, no. 8, pp. 3519–3526, Oct. 1980.

[37] S. Datta, *Electronic Transport in Mesoscopic Systems*. New York: Cambridge Univ. Press, 1995.

[38] D. J. Thouless, "Localization distance and mean free path in one-dimensional disordered systems," *J. Phys. C, Solid State Phys.*, vol. 6, no. 3, pp. L49–L51, Feb. 1973.

[39] A. Yazdanpanah, M. Pourfath, M. Fathipour, H. Kosina, and S. Selberherr, "An analytical model for line-edge roughness limited mobility of graphene nano-ribbons," *IEEE Trans. Electron Devices*, vol. 58, no. 11, pp. 3725–3735, Nov. 2011.

[40] M. Luisier and G. Klimeck, "Performance analysis of statistical samples of graphene nanoribbon tunneling transistors with line edge roughness," *Appl. Phys. Lett.*, vol. 94, no. 22, pp. 223 505-1–223 505-3, Jun. 2009.

Morteza Fathipour (M'90) received the M.S. and Ph.D. degrees in solid-state electronics from Colorado State University, Fort Collins, in 1980 and 1984, respectively.

From 1984 to 1986, he was with Sharif University of Technology, Tehran, Iran. He then joined the Department of Electrical and Computer Engineering, University of Tehran, Tehran, where he is the Founder of the Technology Computer-Aided Design (CAD) Laboratory. His research interests include device physics, semiconductor interface, process/device design, simulation, modeling and characterization for Ultra Large Scale Integration (ULSI) devices, CAD development for process and device design, fabrication of nanodevices, and optoelectronics.

Arash Yazdanpanah received the B.S. degree in electronics from Shahid Bahonar University, Kerman, Iran, in 2000 and the M.S. degree in electronics from Tabriz University, Tabriz, Iran, in 2005. He is currently working toward Ph.D. degree in electronics at Tehran University, Tehran, Iran.

From 2005 to 2007, he was a Design Engineer with the National Iranian Copper Industries Company. His research topics are voltage stability in power networks, fiber Bragg gratings in optical applications, semiconductor devices, and quantum transport in nanostructures.

Hans Kosina (S'89–M'93) received the "Diplomingenieur" degree in electrical engineering and the Ph.D. degree from the Technische Universität Wien, Wien, Austria, in 1987 and 1992, respectively. He received the "venia docendi" in microelectronics in 1998.

For one year, he was with the Institute of Flexible Automation, Technische Universität Wien, where he is currently an Associate Professor with the Institut für Mikroelektronik. In the summer of 1993, he was a Visiting Scientist with Motorola Inc., Austin, TX, and in the summer of 1999, he was a Visiting Faculty with Intel Corporation, Santa Clara, CA. His current research interests include device modeling of semiconductor devices, nanoelectronic devices, organic semiconductors and optoelectronic devices, development of novel Monte Carlo algorithms for classical and quantum transport problems, and computer-aided engineering in ULSI technology.

Mahdi Pourfath (M'08) was born in Tehran, Iran, in 1978. He received the M.S. degree in electrical engineering from Sharif University of Technology, Tehran, in 2002 and the Ph.D. degree in technical sciences from the Technische Universität Wien, Wien, Austria, in 2007.

Since October 2003, he has been with the Institute for Microelectronics, Technische Universität Wien. He is also currently with the Department of Electrical and Computer Engineering, University of Tehran, Tehran. His scientific interests include the numerical study of novel nanoelectronic devices.

Siegfried Selberherr (M'79–SM'84–F'93) was born in Klosterneuburg, Austria, in 1955. He received the Diplomingenieur degree in electrical engineering and the Ph.D. degree in technical sciences from the Technische Universität Wien, Wien, Austria, in 1978 and 1981, respectively. He received the venia docendi on computer-aided design in 1984.

Since 1988, he has been the Chair Professor of the Institut für Mikroelektronik, Technische Universität Wien. From 1998 to 2005, he was the Dean of the Fakultät für Elektrotechnik und Informationstechnik. He published more than 250 papers in journals and books, where more than 80 appeared in the Transactions of the IEEE. He and his research teams achieved more than 750 articles in conference proceedings of which more than 100 have been with an invited talk. He authored two books and coedited 25 volumes, and he supervised, so far, more than 90 dissertations. His current research interests are modeling and simulation of problems for microelectronics engineering.